crystals

MDPI

Article

Distorsion of the $[Ni(OH_2)_6]^{2+}$ Cation in a Benzenesulfonate—Correlation with Hydrogen Bonds or Intra-Cation Interactions?

Ai Wang [1], Adkhamjon Normamatov [2,3,4], Aziz Ibragimov [2], Ulli Englert [5,*], Christian Lehmann [6] and Ruimin Wang [1,*]

1 Institute of Molecular Science, Shanxi University, Taiyuan 030006, China
2 Institute of General and Inorganic Chemistry, Uzbekistan Academy of Sciences, M. Ulugbek Str. 77a, Tashkent 700125, Uzbekistan; adhamjonnormamatov@gmail.com (A.N.)
3 Institute of Bioorganic Chemistry, Uzbekistan Academy of Sciences, Mirzo Ulughbek Str., 83, Tashkent 100125, Uzbekistan
4 Department of Natural Compounds and Applied Chemistry, Faculty of Chemistry, National University of Uzbekistan named after Mirzo Ulugbek, 4 University St., Olmazor, Tashkent 100174, Uzbekistan
5 College of Chemistry and Material Science, Hebei Normal University, Shijiazhuang 050024, China
6 Max-Planck-Institut für Kohlenforschung, Kaiser-Wilhelm-Platz 1, 45470 Mülheim an der Ruhr, Germany; lehmann@mpi-muelheim.mpg.de
* Correspondence: ullrich.englert@ac.rwth-aachen.de (U.E.); ruimindg@qq.com (R.W.)

Abstract

In the absence of electronic reasons for distortion and with its ligands idealized as spherical, the hexaaquanickel(II) cation may be regarded as a simple example for octahedral metal coordination. In structurally characterized derivatives, the cation must adopt a lower symmetry in which it may well be distorted. We investigate hexaaquanickel(II) 3-carboxy-4-hydroxybenzenesulfonate dihydrate, a solid in which the cation occupies a center of inversion and subtends classical O–H···O hydrogen bonds with anions and co-crystallized water. Based on high-resolution X-ray diffraction, we analyze the resulting experimental electron density in order to understand why one of the three independent Ni–O coordinative bonds is significantly shorter than the others. The electron density and its derived properties in the bond critical points do not indicate correlation between hydrogen and coordinative bonds. The electrostatic potential derived from the experimental density reflects the electron distribution in the d orbitals and suggests that intra-cation repulsions and attractions are responsible for the distorsion of the cation. The quality of our experimental results is further underlined by a very good match between the measured electron density in the bond critical points of the Ni–O coordinative bonds and a previous report in the literature.

Keywords: hexaaquacation; high-resolution X-ray diffraction; experimental electron density; aqua ligands; strong hydrogen bonds; electrostatic potential

Check for updates

Academic Editor: Jesús Sanmartín-Matalobos

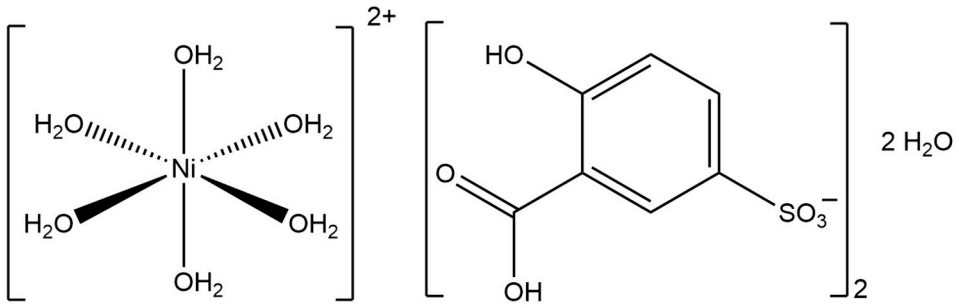
Received: 8 September 2026
Revised: 27 September 2026
Accepted: 28 September 2026
Published: 5 October 2026

Copyright: © 2026 by the authors. Licensee MDPI, Basel, Switzerland. This article is an open access article distributed under the terms and conditions of the Creative Commons Attribution (CC BY) license.

1. Introduction

Aqua complexes of transition metal cations are prototypic species in coordination chemistry. As they represent simple examples for the most popular coordination geometries and their ligand exchange kinetics have been studied in detail [1], they are commonly covered in textbooks [2–5]. In contrast to its higher homologues Pd^{II} and Pt^{II}, the aqua cation of Ni^{II} is hexa-coordinated. If the aqua ligands are perceived as spherical, the cation

is expected to adopt an octahedral structure according to the simple crystal field theory. This expectation is confirmed by diffraction experiments on salts of the $[Ni(OH_2)_6]^{2+}$ cation with symmetric counter anions [6,7] and by calculations on the isolated residue [8,9]. In reality, coordinated water molecules do not represent spherical ligands but dipole molecules with two potential H donor functionalities. Depending on the orientation of the central Ni^{II} with respect to the plane subtended by the three atoms of each aqua ligand, the $[Ni(OH_2)_6]^{2+}$ cation will adopt a lower point symmetry. Potential distorsions of this residue may therefore have two different reasons: On the one hand, the peripheric hydrogen atoms may interact with suitable acceptors in a less symmetric fashion. Siegler et al. [10,11] and Lacroix et al. [12] noted that discrepancies from the idealized regular octahedral geometry correlate with the environment about the hexaaquacations in the crystal. On the other hand, a low symmetry arrangement of the six aqua ligands may result in repulsive and attractive electrostatic interactions within the $[Ni(OH_2)_6]^{2+}$ cation and cause distorsions. Obviously, both effects may contribute to the observed arrangement within the cation. Even for high-quality diffraction experiments, such observations are exclusively based on geometric arguments such as interatomic distances and angles. In the present study, we go beyond this entirely geometric approach and also consider the associated electron density derived from a high-resolution diffraction experiment and an atom-centered multipole refinement. For this purpose, we selected hexaaquanickel(II) 3-carboxy-4-hydroxybenzenesulfonate dihydrate, **1** (Scheme 1).



Scheme 1. Chemical diagram of hexaaquanickel(II) 3-carboxy-4-hydroxybenzenesulfonate dihydrate, **1**.

Experimental electron density studies based on high-resolution X-ray diffraction are still rather rare, and we are not aware of a comparable hexaaquacation investigated by the same method. We note that an X-ray diffraction experiment of **1** at 150 K and standard resolution was conducted by Bettinger et al. [13]. An additional benefit of high-resolution diffraction experiments lies in the fact that standard uncertainties are about 10 times smaller than those of a competently conducted structure determination at the usual resolution of $(\sin\theta/\lambda)_{max} = 0.7$ Å^{-1}.

2. Materials and Methods

We report here our original synthesis, although the reagent monoethanolamine is not incorporated into the product. Two solutions were prepared separately. Solution 1: 5-sulfosalicylic acid dihydrate (1 mmol, 0.254 g) was dissolved in ethanol (20 mL). Monoethanolamine (1 mmol, 61 µL) was added and mixed thoroughly, resulting in a pH of 3.8. Solution 2: $NiCl_2 \cdot 4H_2O$ (0.5 mmol, 0.101 g) was dissolved in water (15 mL). Solution 1 was then added slowly to solution 2 and mixed, resulting in a pH of 4.1. The target compound was obtained by slow evaporation of the solvents over a period of 12 days in a constant temperature chamber kept at 22 °C; yield 70% (based on $NiCl_2 \cdot 4H_2O$ or 5-sulfosalicylic acid dihydrate). Analysis % found (calc for $C_{14}H_{26}NiO_{20}S_2$) C 25.89 (26.39);

H 4.02 (4.11); S 9.98 (10.07); O 50.07 (50.22). Salt **1** was further characterized by UV/vis and IR spectroscopy; these results have been compiled in the Supplementary Materials. The crystalline bulk contained single crystals suitable for X-ray diffraction. Bettinger et al. [13] reported the synthesis of **1** without monoethanolamine.

For scaling and deconvolution of displacement parameters and non-spherical electron density in the valence shell, experimental electron density studies require complete and highly redundant intensity data collected at low temperature and up to high resolution. Well-defined occupancies for the scattering centers are mandatory for the reliable refinement of atom-centered multipoles; therefore crystals should not only be "ideally imperfect" [14] but also free of disorder. As elevated redundancy and high resolution result in prolonged intensity data collections, the target crystals must be sufficiently stable. Salt **1** forms light green block-shaped crystals of good quality and suitable dimensions for diffraction experiments. Preliminary tests showed that the oxygen atom of the co-crystallized water molecule is associated with a displacement parameter similar to those encountered for the aqua ligands and that the crystals do not undergo any phase transition between ambient temperature and 100 K. Intensity data were measured at 100 K (Oxford Cryosystems Ltd., Oxford, UK) with MoKα radiation generated by a Nonius FR591 rotating anode (Enraf-Nonius, Delft, The Netherlands). A Nonius Kappa diffractometer (Enraf-Nonius, Delft, The Netherlands) equipped with an Incoatec mirror and an Apex 2 CCD detector (Bruker, Madison, WI, USA) was used for data collection.

Crystal data, data collection parameters and convergence results have been compiled in Table 1. CIF files for the Independent Atom Model (IAM) and the Multipolar Model (MM) refinement of **1** have been deposited with the Cambridge Structural Database under the deposition numbers 2492162 (IAM) and 2492163 (MM). The result of the conventional refinement [15] with spherical scattering factors was used as starting geometry for the multipolar refinement with XD2016 [16]. It was conducted with all intensity data $I > 0$ and with anisotropic displacement parameters for the hydrogen atoms obtained from the SHADE server [17,18]. The final MM refinements on F^2 comprised multipoles up to hexadecapoles for non-H atoms, up to bond-directed dipoles for the carbon-bonded H atoms and up to quadrupoles for the H atoms bonded to oxygen. For Ni, the z axis was chosen in the direction of O2; y and x axes almost coincide with the vectors from the metal cation to O1 and O3, respectively. Contraction parameters were refined freely, starting with a value of 2.0 for Ni; $\varkappa'$ for the H atoms was fixed to 1.2. Contraction parameters and monopole population coefficients have been compiled in Table S6. The positional parameters of all H atoms were refined freely.

Table 1. Crystal data, data collection parameters and convergence results for **1**.

Crystal Data	
Chemical formula	$C_{14}H_{26}NiO_{20}S_2$
Mr	637.16
Crystal system, space group	triclinic, *P*-1
Temperature (K)	100(2)
a (Å)	6.5784(3)
b (Å)	7.3916(9)
c (Å)	13.2645(7)
α (°)	74.252(6)
β (°)	88.589(5)
γ (°)	77.892(6)
V (Å^3)	606.61(8)
Z	1
Radiation type, wavelength (Å)	Mo$K\alpha$, 0.71073

Table 1. *Cont.*

Crystal Data		
μ (mm^{-1})	1.065	
Crystal size (mm)	0.30 × 0.25 × 0.25	
Data Collection		
Diffractometer	Bruker AXS ENRAF-Nonius KappaCCD	
Absorption correction	Gaussian integration, followed by multi-scan correction	
T_{min}, T_{max}	0.781, 0.861	
Measured reflections	108,434	
Independent reflections	17,561	
Observed reflections	15,967	
R_{int}	0.0245	
$(\sin\theta/\lambda)_{max}$ (Å^{-1})	1.21	
Refinement	**IAM**	**MM**
R_1	0.0266	0.0164
wR_2	0.0761	0.0469
GOF	1.149	0.993
No. of reflections	17,461	17,059
No. of parameters	209	775
$\Delta\rho_{max}$, $\Delta\rho_{min}$ (eÅ^{-3})	2.09 [1], −0.47	0.46, −0.38

[1] The high residual maximum is a consequence of high resolution; for data truncated at standard resolution $(\sin\theta/\lambda)_{max}$ = 0.7 Å^{-1}, $\Delta\rho_{max}$ = 0.5 eÅ^{-3} and $\Delta\rho_{min}$ = −0.4 eÅ^{-3}.

3. Results

3.1. Geometry

Salt **1** crystallizes in the triclinic space group *P*-1, with a $[Ni(OH_2)_6]^{2+}$ dication on a center of inversion and a benzenesulfonato anion as well as a co-crystallized water molecule in general positions. For consistency, all numerical data and graphical results refer to the multipole refinement; see Section 3.2. Figure 1 shows a displacement ellipsoid plot and the atom numbering scheme.

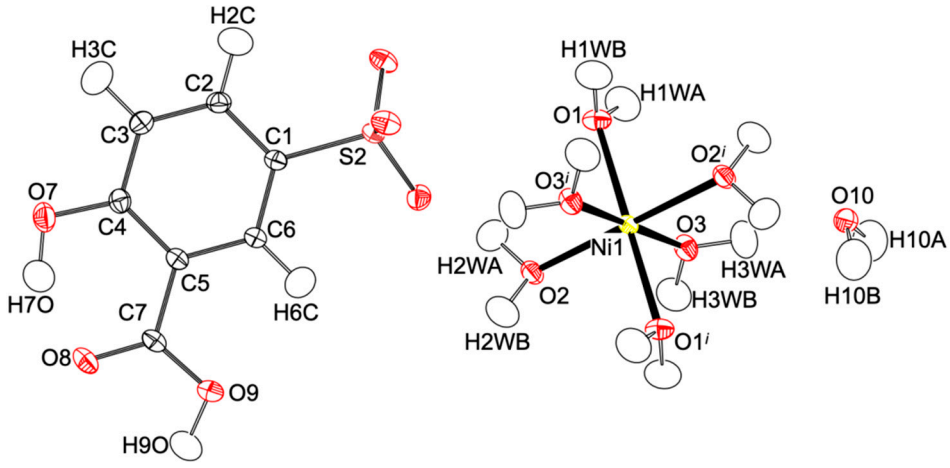


Figure 1. Displacement ellipsoid plot (70% probability) for **1**; symmetry operator: ^{i} = 1 − x, 1 − y, 1 − z. Anisotropic displacement parameters for hydrogen atoms were obtained from the SHADE server [17,18], cf. Supplementary Materials.

In the crystal, the residues segregate according to their hydrophilicity and thus allow for specific interactions. Figure 2 shows a projection of the unit cell along [0 1 0]. Regions dominated by stacking and hydrogen-bonded areas alternate along [0 0 1]. Stacking occurs between hydrophobic aromatic rings of neighboring sulfonato anions and involves C···C contacts as short as 3.2 Å; these regions have been marked with a yellow background in

Figure 2. Hydrogen bonds (see Table 2) dominate the hydrophilic regions marked with a blue background.

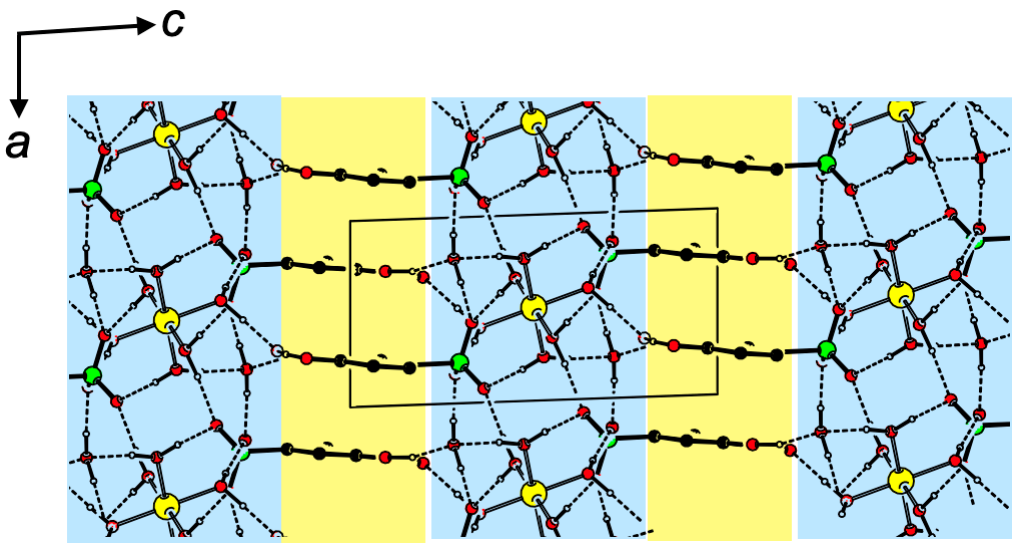


Figure 2. Packing pattern in **1**; regions with dominating classical hydrogen bonds (HBs) have been marked by a blue and those with stacking by a yellow background. HBs are shown as dashed lines, H atoms not involved in classical HBs have been omitted.

One important aspect of our study is the potential correlation between the classical hydrogen bonds (HBs, Table 2) and the coordination environment about the Ni^{II} center (Table 3); additional interatomic distances and angles are provided in the CIFs.

In the absence of other electronegative atoms, classical HBs are exclusively of the O–H···O type. Not surprisingly, all eleven H atoms in the asymmetric unit which are attached to oxygen find an acceptor atom at suitable distance. With the exception of the only intramolecular HB, the donor–H···acceptor angle is larger than 160°. The oxygen atoms O1, O2 and O3 of the aqua ligands do not act as HB acceptors. The only intramolecular HB (O7–H7O···O8) is part of a six-membered ring. The donor acceptor distance of 2.58 Å is longer than in the case of the well-studied acetylacetonates on which neutron diffraction experiments have been conducted [19–21].

Table 2. Donor–hydrogen···acceptor (D–H···A) geometry for classical hydrogen bonds in **1**.

D–H···A	D–H [Å]	H···A [Å]	D···A [Å]	Angle D–H···A [°]
O1–H1WA···O6 ^{i}	1.024(12)	1.821(12)	2.8419(5)	173.9(9)
O1–H1WB···O5 ^{ii}	0.997(13)	1.781(13)	2.7740(5)	173.2(11)
O2–H2WA···O4	1.021(12)	1.799(12)	2.7802(5	160.1(9)
O2–H2WB···O8 ^{iii}	1.026(12)	1.729(12)	2.7361(5)	166.0(11)
O3–H3WA···O10	1.017(12)	1.802(12)	2.8126(4)	172.1(10)
O3–H3WB···O6 ^{iv}	1.000(13)	1.872(13)	2.8686(5)	174.0(12)
* O7–H7O···O8	1.021(13)	1.671(13)	2.5800(5)	145.7(11) *
O9–H9O···O10 ^{v}	1.046(13)	1.635(13)	2.6573(4)	164.5(12)
O10–H10A···O4 ^{vi}	1.028(14)	1.783(14)	2.7950(5)	167.2(12)
O10–H10B···O5 ^{vii}	1.006(13)	1.724(13)	2.7300(5)	178.2(12)

Symmetry operators: ^{i} = −x, 2 − y, 1 − z; ^{ii} = 1 − x, 2 − y, 1 − z; ^{iii} = 1 − x, 1 − y, 2 − z; ^{iv} = x, −1 + y, z; ^{v} = x, y, 1 + z; ^{vi} = −x, 1 − y, 1 − z; ^{vii} = 1 − x, 1 − y, 1 − z. * Intramolecular hydrogen bond.

Table 3 shows that the cation is slightly distorted. The quadratic elongation amounts to only 1.001 and the angle variance to 3.25 deg^2. [22] We had structurally characterized an almost regular hexaaquanickel(II) cation in the form of its nitrobenzoate dihydrate [23].

In this previously reported structure, the cation is also located on a center of inversion, with Ni–O bond distances between 2.0351(17) and 2.080(2) Å, but the corresponding diffraction experiment had been conducted at ambient temperature and standard resolution: standard uncertainties were larger as in the present case, and no experimental electron density study was attempted. In contrast, the distorsion encountered in the cation of **1** amounts to more than 50 standard uncertainties and therefore must be regarded as statistically significant.

Table 3. Coordinative bonds and angles in the $[Ni(OH_2)_6]^{2+}$ dication.

Coordination Distances [Å]	Coordination Angles [°]	Coordination Angles [°]
Ni1–O1 = 2.04983(19)	O1–Ni1–O2 = 88.839(8)	O1–Ni1–O3 ^{vii} = 91.909(8)
Ni1–O2 = 2.03832(17)	O1–Ni1–O2 ^{vii} = 91.161(8)	O2–Ni1–O3 = 88.056(8)
Ni1–O3 = 2.05268(18)	O1–Ni1–O3 = 88.091(8)	O2–Ni1–O3 ^{vii} = 91.944(8)

Symmetry operator: ^{vii} = 1 − x, 1 − y, 1 − z.

The distance between Ni and oxygen O2 is significantly shorter than Ni1-O1 and Ni1-O3. The earlier diffraction experiment on **1** at standard resolution [13] agrees with this trend. If the complex cation, the molecular anions and the co-crystallized water molecule are perceived as independent residues, the most relevant directional interactions between these building blocks are doubtlessly hydrogen bonds. A correlation between Ni-O and classical, presumably strong, hydrogen bonds might well exist. A first inspection of Tables 2 and 3 in terms of distances does not suggest an obvious correlation of this kind for **1**: The aqua ligand O2 closest to the Ni(II) cation is neither involved in the shortest nor in the longest HBs. At second sight, the last column in Table 2 indicates that O2 acts as donor for less linear HBs than the other aqua ligands. Our diffraction data collected on **1** allow for an analysis beyond geometry: The electron density is an observable which may directly be recovered via high-resolution X-ray diffraction. As excellent crystals of **1** were available and neither the earlier report by Bettinger et al. [13] nor our own preliminary experiments at 100 K indicated disorder, hydrate instability or any unwelcome phase transition, we decided to perform such an experiment to measure the electron density and its derived properties. The electron density can help to decide whether correlation with hydrogen bonds or intra-cation interactions are responsible for the experimentally observed distorsion of the $[Ni(OH_2)_6]^{2+}$ cation: As for the former alternative, HBs are secondary interactions with a strong electrostatic contribution. With respect to the second alternative, the electrostatic potential (ESP) can be expected to provide information concerning potential intra-cation repulsions and attractions.

3.2. Experimental Electron Density

After convergence of the multipole refinement, the resulting experimental electron density was analyzed with Bader's QTAIM approach [24]. All covalent, coordinative bonds and classical hydrogen bonds are associated with bond critical points (bcps), thus providing a good check for the reliability of the high-resolution data; a full list of bcps is provided in the Supplementary Materials. As an example, Figure 3 shows a trajectory plot of the gradient of the electron density with critical points in the sulfonato fragment; such a flat residue is particularly well-suited for a static image in two dimensions.

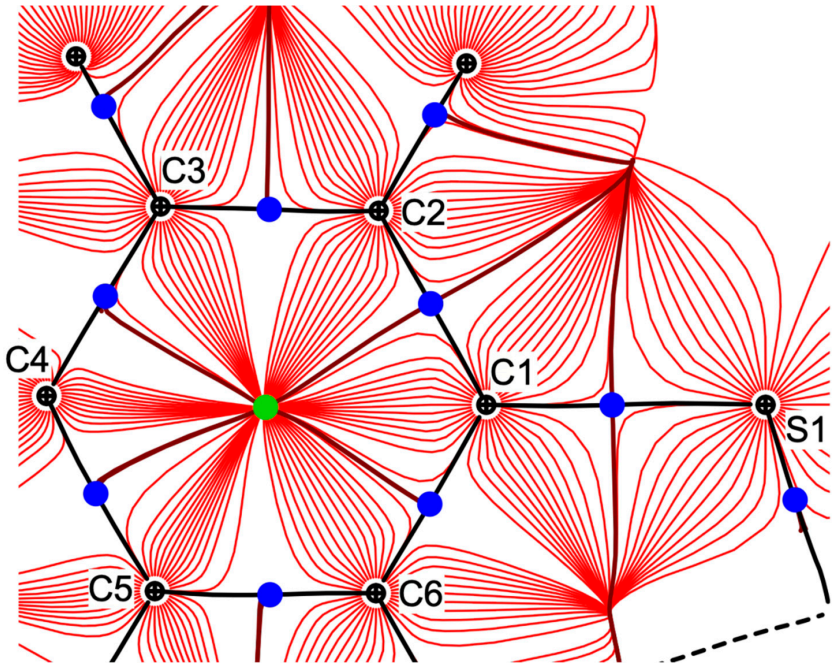


Figure 3. Atomic basin paths of the gradient of the experimental electron density; bond paths are shown as black lines. Nuclear attractors are depicted as white, bcps as dark blue and the ring critical point as green solid circles.

According to the simple crystal field (CF) model, the electron configuration d^8 for the central Ni^{II} in the hexaaquacation implies fully occupied t_{2g} (d_{xy}, d_{xz} and d_{yz}) orbitals pointing in between the ligands and single occupancy of the e_g orbitals in the direction of octahedral coordination [25]. The results of our experimental electron density determination match the expectations of this model very well. Figure 4 shows the electrostatic potential (ESP) mapped on an isosurface of the Laplacian of the electron density: the charge accumulations at the O atoms of the aqua ligands directed towards the cation are clearly visible.

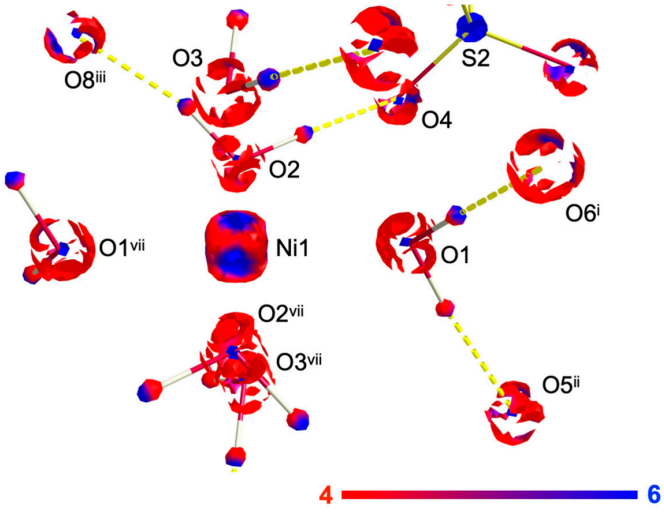


Figure 4. ESP mapped on a Laplacian isosurface (-80 eA^{-5}, program MoleCoolQt [26]). Note that at such a surface close to the nuclei, all ESP are positive; the color code reflects the differences. For symmetry operators, see Table 2. Dashed yellow lines represent HBs.

Figure 4 shows not only the polarization of the coordinating O atoms by the Ni cation but also the charge accumulations pointing in between the aqua ligands; the CF model

interprets these charge accumulations as the fully occupied t_{2g} orbitals. When the total number of d electrons at Ni is scaled to match the CF-predicted electron configuration d^8, the experimental electron density associates the e_g orbitals oriented towards the ligands with 1.2 and those of the t_{2g} orbitals with 1.8–1.9 electrons; the numerical values are provided in the Supplementary Materials.

The obvious criteria for judging quality and strength of a bond or short contact based on the associated electron density are properties in the bcp, foremost the electron density ρ and its Laplacian. Table 4 summarizes the results of the topological analysis of the electron density which are relevant for a possible correlation between coordinative and hydrogen bonds.

The top part of Table 4 gives details of the electron density and its derived properties for those hydrogen bonds involving aqua ligands as HB donors. The second part of the table is devoted to the remaining hydrogen bonds without the participation of aqua ligands as donors. The electron density in the bcps for the intermolecular O–H···O interactions matches the expectation for classical HBs between 2.6 and 2.9 Å [27,28]. The Laplacian in the bcps adopts small positive values or, in one case, a value close to zero within standard uncertainties. Such behavior has been reported by Munshi and Row [29].

The last section of Table 4 refers to the coordinative bonds between the Ni^{II} cation and the oxygen atoms of the aqua ligands. The electron densities in the three crystallographically independent Ni-O bonds are equal within a few standard uncertainties. A theoretical study of the hexaaquanickel(II) cation, followed by a QTAIM analysis of the electron density, found 0.057 ea_0^{-3} (in atomic units, corresponding to 0.385 $eÅ^{-3}$) for the bcps in these bonds [9], in excellent agreement with our experimentally observed values.

Table 4. Properties of the electron density in the bcps of hydrogen and coordinative bonds in **1**. For interactions subtended by atoms 1 and 2 in the first column, d_1 is the distance of the first atom to the bond critical point, R_{12} the sum of the distances of atoms 1 and 2 to the bond critical point, ∇^2 the Laplacian in the bcp, G the kinetic, V the potential and E the total energy density.

Bond	R_{12}	d_1	ρ	∇^2	G	V	E
	[Å]	[Å]	[$eÅ^{-3}$]	[$eÅ^{-5}$]	[au]	[au]	[au]
H1WA···O6 ^{i}	1.8257	0.5595	0.16(4)	1.6(2)	0.0163	−0.0163	0
H1WB···O5 ^{ii}	1.7855	0.5555	0.25(5)	−0.4(2)	0.0094	−0.0224	−0.013
H2WA···O4	1.8466	0.5522	0.12(5)	2.0(2)	0.017	−0.0135	0.0035
H2WB···O8 ^{iii}	1.831	0.5601	0.09(5)	2.8(2)	0.0213	−0.0137	0.0075
H3WA···O1	1.8035	0.5031	0.16(6)	4.8(2)	0.0387	−0.0274	0.0113
H3WB···O6 ^{iv}	1.876	0.5955	0.14(7)	1.8(2)	0.0168	−0.0151	0.0018
* H7O···O8	1.7489	0.5888	0.18(5)	4.6(2)	0.0389	−0.0298	0.0091 *
H9O···O10 ^{v}	1.6989	0.4848	0.20(7)	4.9(2)	0.0421	−0.0332	0.0088
H10A···O4 ^{vi}	1.7903	0.5296	0.18(6)	1.4(2)	0.0164	−0.0181	−0.0017
H10B···O5 ^{vii}	1.8196	0.5776	0.15(5)	2.2(2)	0.0203	−0.018	0.0023
Ni1–O1	2.051	0.9917	0.384(6)	11.672(9)			
Ni1–O2	2.0385	0.9872	0.391(6)	11.985(8)			
Ni1–O3	2.053	0.9923	0.375(6)	11.576(8)			

See Table 2 for symmetry operators and additional geometry details. * Intramolecular hydrogen bond.

Energy density considerations may be helpful to categorize secondary interactions. The kinetic energy density G was derived as suggested by Abramov [30], and the potential energy density V was obtained according to the local virial theorem [31,32]. The total energy density E, the sum of the (positive) kinetic energy density G and the (negative) potential energy density V, represents a useful tool for the analysis of short contacts. It assumes negative values for covalent bonds [33] and only for the shortest hydrogen bonds [28], and Cl···Cl contacts [34], whereas, in general, values close to zero are encountered for secondary interactions.

4. Discussion

Based on the accurate geometry data compiled in Tables 2 and 3 and the results of the experimental electron density determination listed in Table 4, we can discuss possible reasons for the cation distorsion. The significantly shorter Ni–O bond in the coordination sphere about Ni^{II} is associated with the oxygen atom O2. We will first investigate potential correlations between coordinative and hydrogen bonds. The electron densities in the HBs involving O2 as donor appear to be the lowest, but this sequence is not significant in view of the standard uncertainties. None of the other listed properties, neither the Laplacian of the electron density nor the total energy density in the bcp and its individual energy density contributions *G* or *V*, assume extreme values for the interactions involving O2. In a synopsis of all criteria, only the interaction O1–H1WB···O5 ^{ii} stands out: although it does not reflect the shortest hydrogen bond in **1**, it is associated with the shortest bond path and the highest ρbcp. It also represents the only HB with a negative Laplacian and a significantly negative overall energy density E in the bond critical point. It is tempting to address this hydrogen bond as the strongest among those relevant for the $[Ni(OH_2)_6]^{2+}$ coordination environment. We note, however, that the second HB subtended by the same aqua ligand is unexceptional. We therefore conclude that no straightforward correlation between coordinative and hydrogen bonds can be detected in **1**.

Intra-cation interactions represent an alternative reason for distorsion. In the aqua ligands, the three atoms of each coordinated water molecule and the central Ni^{II} are not coplanar. The $[Ni(OH_2)_6]^{2+}$ cation can therefore not adopt (local) T_h point symmetry with double and triple degenerate *d* orbitals. The crystallographically imposed C_i symmetry allows for three different Ni–O distances and six independent O···O edges in the NiO_6 polyhedron; these O···O distances vary between 2.84 and 2.95 Å. Figure 5 shows the electrostatic potential (ESP) about the aqua ligands in the cation, mapped on an electron density isosurface. This presentation emphasizes the regions of opposite charge in the coordinated water molecules.

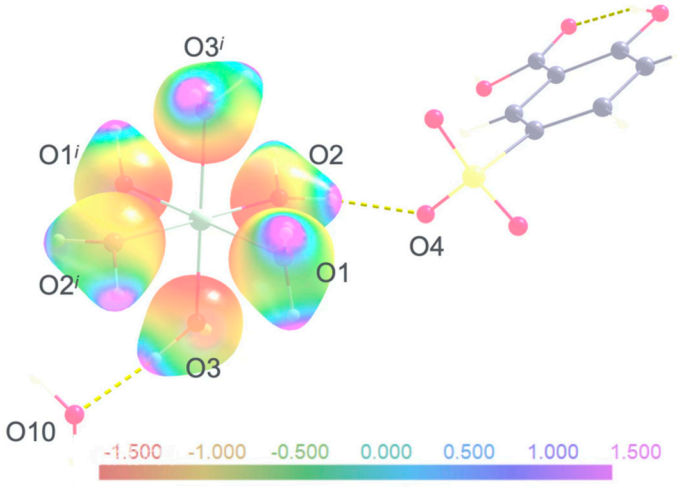


Figure 5. Electrostatic potential of the aqua ligands in the cation of **1**, mapped on an electron density isosurface of 0.5 eÅ^{-3} (program MoleCoolQt [21]). Dashed lines repesent HBs. Symmetry operator ^{i} = 1 − x. 1 − y, 1 − z.

The ESP confirms chemical intuition: the Ni-coordinated oxygen atoms of the aqua ligands are associated with a negative and H atoms with a positive potential. The overall geometry of the cation must not only balance Ni–O but also presumably attractive H···O and repulsive O···O and H···H interactions. We here only mention that for O2, the target

atom of the shortest Ni–O bond, the shortest H···O contact is 0.14 Å longer than that for O1 and O3.

5. Conclusions

We have discussed two potential reasons for the statistically significant distorsion of the $[Ni(OH_2)_6]^{2+}$ cation in **1**. The experimentally observed electron density does not suggest a clear correlation between coordinative and hydrogen bonds in this compound. The picture provided by the ESP shows that the symmetry of the cation cannot be idealized as octahedral: not only the Ni–O bonds but also the shortest O···O, O···H and H···H distances cover a relevant range. In view of the fact that these interactions must essentially be perceived as electrostatic, their influence even at slightly longer distances around 2.8 Å cannot be ignored. We conclude that a subtle balance between coordinative bonds on the one hand and intra-cation attractions and repulsions on the other hand is decisive for the observed distorsion; the moderately strong HBs may well contribute to the orientation of the individual aqua ligands.

Supplementary Materials: The following supporting information can be downloaded at: https://www.mdpi.com/article/10.3390/cryst16100637/s1, Figure S1: Spectra of solutions of **1** in the concentration range between 0.1 M and 0.7 M show the presence of the nickelhexaaqua cation; Figure S2: UV absorption maxima characteristic for the organic anion in **1**; Figure S3: IR spectrum of sulfosalicylic acid; Figure S4: IR spectrum of **1** [35,36]; Figure S5: Scatterplot for X-ray refinement result (MM) for **1**; Figure S6: Probabillity distribution histogram of residual electron density of **1**; Figure S7: Fractal dimension plot of residual electron density of **1**; Figure S8: Residual electron density (MM) of **1**, on isosurfaces of $\rho = 0.17$ e·Å^{-3} and $\rho = -0.17$ e·Å^{-3}; Figure S9: Deformation density ρMM-ρIAM of **1**, on isosurfaces of $\rho = 0.23$ e·Å^{-3} and $\rho = -0.23$ e·Å^{-3}; Table S1: Resolution and completeness statistics (cumulative and Friedel pairs averaged) of **1**; Table S2: R-value statistics as a function of resolution (in resolution shells) of **1**; Table S3: Final Coordinates and equivalent isotropic displacement parameters of the atoms in **1**; Table S4: Anisotropic displacement parameters of the non-hydrogen atoms in **1**; Table S5: Anisotropic displacement parameters of the hydrogen atoms in the **1**; Table S6: Monopole populations, radial parameters and net atomic charges for atoms in **1**; Table S7: Topological properties of interactions at their bond critical point (3,−1); Table S8: *d* orbital population at Ni^{II} in **1**, assuming an overall d^8 electron configuration.

Author Contributions: Conceptualization, A.I., R.W. and U.E.; methodology, R.W. and C.L.; validation, A.W., R.W. and U.E.; formal analysis, A.W. and A.I.; investigation, A.W. and A.N.; resources, A.I. and C.L.; data curation, A.W.; writing—original draft preparation, U.E.; writing—review and editing, all authors; visualization, A.W. and R.W.; supervision, R.W. and U.E.; project administration, A.W., R.W. and U.E.; funding acquisition, A.W. and U.E. All authors have read and agreed to the published version of the manuscript.

Funding: This research was funded by the Shanxi Scholarship Council of China, grant number 2023-018, and the program of the State Key Laboratory of Quantum Optics Technologies and Devices, grant number 202502.

Data Availability Statement: Diffraction data for **1** and their derived results have been deposited in CIF format with the CCDC under deposition numbers 2492162 (IAM) and 2492163 (MM). Other data presented in this study are available on request from the corresponding authors.

Acknowledgments: This work was supported financially by the Shanxi Scholarship Council of China (2023-018) and the program of the State Key Laboratory of Quantum Optics Technologies and Devices (Grant No. 202502).

Conflicts of Interest: The authors declare no conflicts of interest.

Abbreviations

The following abbreviations are used in this manuscript:

CF	Crystal Field
ESP	Electrostatic Potential
IAM	Independent Atom Model
MM	Multipolar Model
QTAIM	Quantum Theory of Atoms in Molecules

References

1. Lincoln, S.F.; Richens, D.T.; Sykes, A.G. Metal Aqua Ions. In *Comprehensive Coordination Chemistry II*, 2nd ed.; McCleverty, J.A., Meyer, T.J., Eds.; Elsevier: Amsterdam, The Netherlands, 2003; Volume 1, pp. 515–555.
2. Huheey, J.E.; Keiter, E.A.; Keiter, R.L.; Medhi, O.K. *Inorganic Chemistry: Principles of Structure and Reactivity*, 4th ed.; Harper Collins College Publishers: New York, NY, USA, 1993.
3. Weber, B. *Coordination Chemistry, Basics and Current Trends*; Springer: Berlin, Heidelberg, Germany, 2023. [CrossRef]
4. Janiak, C.; Meyer, H.-J.; Gudat, D.; Kurz, P. *Riedel Moderne Anorganische Chemie*; De Gruyter: Berlin, Germany; Boston, MA, USA, 2018. [CrossRef]
5. Geoffrey, A.L. *Introduction to Coordination Chemistry*, 1st ed.; John Wiley & Sons, Ltd.: Hoboken, NJ, USA, 2010.
6. Blackburn, A.C.; Gallucci, J.C.; Gerkin, R.E. Structure of hexaaquanickel(II) bromate. *Acta Crystallogr. C* **1991**, *47*, 1786–1789. [CrossRef] [PubMed]
7. Gallucci, J.C.; Gerkin, R.E. The structure of hexaaquanickel(II) chlorate. *Acta Crystallogr. C* **1990**, *46*, 350–354. [CrossRef] [PubMed]
8. Kenji, W.; Hitoshi, O.; Hideki, M.; Nobuhiro, F.; Youichi, W. Density Functional Calculation on the Geometries and Dissociation Energies of $[M(H_2O)_6]^{2+}$ Ions. M^{2+} = Cr^{2+}, Mn^{2+}, Fe^{2+}, Co^{2+}, Ni^{2+}, Cu^{2+}, and Zn^{2+}. *Chem. Lett.* **1992**, *8*, 1489–1492. [CrossRef]
9. Conradie, J. Jahn-Teller effect in high spin d^4 and d^9 octahedral metal-complexes. *Inorganica Chim. Acta* **2019**, *486*, 193–199. [CrossRef]
10. Siegler, M.A.; Hao, X.; Parkin, S.; Brock, C.P. $[Ni(H_2O)_6](NO_3)_2 \cdot$(15-crown-5)$\cdot 2H_2O$: Three phase transitions and an intermediate modulated phase stable over a range of ca 40 K. *Acta Crystallogr. B* **2011**, *67*, 486–498. [CrossRef] [PubMed]
11. Siegler, M.A.; Parkin, S.; Selegue, J.P.; Brock, C.P. The elusive $[Ni(H_2O)_2$(15-crown-5)$]^{2+}$ cation and related co-crystals of nickel(II) hydrates and 15-crown-5. *Acta Crystallogr. B* **2008**, *64*, 725–737. [CrossRef] [PubMed]
12. Lacroix, M.R.; Bukovsky, E.v.; Lozinšek, M.; Folsom, T.C.; Newell, B.S.; Liu, Y.; Peryshkov, D.v.; Strauss, S.H. Manifestations of Weak O-H···F Hydrogen Bonding in $M(H_2O)_n(B_{12}F_{12})$ Salt Hydrates: Unusually Sharp Fourier Transform Infrared ν(OH) Bands and Latent Porosity (M = Mg-Ba, Co, Ni, Zn). *Inorg. Chem.* **2018**, *57*, 14983–15000. [CrossRef] [PubMed]
13. Bettinger, R.T.; Squattrito, P.J.; Aulakh, D.; Gianopoulos, C.G.; Mague, J.T. Crystal structures of two new divalent transition-metal salts of carboxybenzenesulfonate anions. *Acta Crystallogr. E* **2022**, *78*, 961–965. [CrossRef] [PubMed]
14. Kato, N. On Extinction. I. General Formulation. *Acta Crystallogr. A* **1976**, *32*, 453–457. [CrossRef]
15. Sheldrick, G.M. Crystal structure refinement with SHELXL. *Acta Crystallogr. C* **2015**, *71*, 3–8. [CrossRef] [PubMed]
16. Volkov, A.; Macchi, P.; Farrugia, L.J.; Gatti, C.; Mallinson, P.; Richter, T.; Koritsanszky, T. *XD2016, A Computer Program Package for Multipole Refinement, Topological Analysis of Charge Densities and Evaluation of Intermolecular Energies from Experimental and Theoretical Structure Factors*; University of Glasgow: Glasgow, UK, 2016.
17. Madsen, A.Ø. SHADE web server for estimation of hydrogen anisotropic displacement parameters. *J. Appl. Crystallogr.* **2006**, *39*, 757–758. [CrossRef]
18. Madsen, A.Ø.; Hoser, A.A. SHADE3 server: A streamlined approach to estimate H-atom anisotropic displacement parameters using periodic ab initio calculations or experimental information. *J. Appl. Crystallogr.* **2014**, *47*, 2100–2104. [CrossRef]
19. Piccoli, P.M.B.; Koetzle, T.F.; Schultz, A.J.; Zhurova, E.A.; Stare, J.; Pinkerton, A.A.; Eckert, J.; Hadzi, D.J. Variable temperature neutron diffraction and X-ray charge density studies of tetraacetylethane. *J. Phys. Chem. A* **2008**, *112*, 6667–6677. [CrossRef] [PubMed]
20. Truong, K.-N.; Merkens, C.; Meven, M.; Faßbänder, B.; Dronskowski, R.; Englert, U. Phase transition and proton ordering at 50 K in 3-(pyridin-4-yl) pentane-2, 4-dione. *Struct. Sci.* **2017**, *73*, 1172–1178. [CrossRef]
21. Truong, K.-N.; Meven, M.; Englert, U. Proton disorder in a short intramolecular hydrogen bond investigated by single-crystal neutron diffraction at 2.5 and 170 K. *Cryst. Struct. Commun.* **2018**, *74*, 1635–1640. [CrossRef] [PubMed]
22. Robinson, K.K.; Gibbs, G.V.; Ribbe, P.H. Quadratic Elongation: A Quantitative Measure of Distortion in Coordination Polyhedra. *Science* **1971**, *172*, 567–570. [CrossRef] [PubMed]
23. Ibragimov, A.B.; Englert, U.; Ashurov, J.M.; Wang, A. Dimorphism of Hexaaquanickel (Ii) Bis (p-Nitrobenzoate) Dihydrate Salt: A New Triclinic Crystal Form. *J. Struct. Chem.* **2018**, *59*, 411–414. [CrossRef]

24. Bader, R.F.W. *Atoms in Molecules—A Quantum Theory*; Clarendon Press: Oxford, UK, 1990.
25. Gispert, J.R. *Coordination Chemistry*; Wiley-VCH: Weinheim, Germany, 2008.
26. Hübschle, C.B.; Dittrich, B. MoleCoolQt—A molecule viewer for charge-density research. *J. Appl. Crystallogr.* **2011**, *44*, 238–240. [CrossRef] [PubMed]
27. Mata, I.; Alkorta, I.; Molins, E.; Espinosa, E. Universal Features of the Electron Density Distribution in Hydrogen Bonding Regions: A Comprehensive Study Involving H···X (X=H, C, N, O, F, S, Cl, p) Interactions. *Chem. Eur. J.* **2010**, *16*, 2442–2452. [CrossRef] [PubMed]
28. Şerb, M.; Wang, R.; Meven, M.; Englert, U. The whole range of hydrogen bonds in one crystal structure: Neutron diffraction and charge-density studies of N,N-dimethylbiguanidinium bis(hydro gensquarate). *Acta Crystallogr. B* **2011**, *67*, 552–559. [CrossRef] [PubMed]
29. Munshi, P.; Guru Row, T.N. Charge density based classification of intermolecular interactions in molecular crystals. *CrystEngComm* **2005**, *7*, 608–611. [CrossRef]
30. Abramov, Y.A. On the Possibility of Kinetic Energy Density Evaluation from the Experimental Electron-Density Distribution. *Acta Crystallogr. A* **1997**, *53*, 264–272. [CrossRef]
31. Espinosa, E.; Molins, E.; Lecomte, C. Hydrogen bond strengths revealed by topological analyses of experimentally observed electron densities. *Chem. Phys. Lett.* **1998**, *285*, 170–173. [CrossRef]
32. Espinosa, E.; Lecomte, C.; Molins, E. Experimental electron density overlapping in hydrogen bonds: Topology vs. Energetics. *Chem. Phys. Lett.* **1990**, *300*, 745–748. [CrossRef]
33. Cremer, D.; Kraka, E. Chemical Bonds without Bonding Electron Density—Does the Difference Electron-Density Analysis Suffice for a Description of the Chemical Bond? *Angew. Chem. Int. Ed.* **1984**, *23*, 627–628. [CrossRef]
34. Wang, A.; Wang, R.; Kalf, I.; Dreier, A.; Lehmann, C.W.; Englert, U. Charge-Assisted Halogen Bonds in Halogen-Substituted Pyridinium Salts: Experimental Electron Density. *Cryst. Growth Des.* **2017**, *17*, 2357–2364. [CrossRef]
35. Liu, W.; Migdisov, A.; Williams-Jones, A. The stability of aqueous nickel (II) chloride complexes in hydrothermal solutions: Results of UV–Visible spectroscopic experiments. *Geochim. Cosmochim. Acta* **2012**, *94*, 276–290. [CrossRef]
36. Rasyda, Y.A.; Rahardjo, S.B.; Nurdiyah, F. Synthesis and characterization complex nickel (II) with diphenylamine. In *IOP Conference Series: Materials Science and Engineering*; IOP Publishing: Bristol, UK, 2019; Volume 578, No. 1, p. 012008. [CrossRef]

Disclaimer/Publisher's Note: The statements, opinions and data contained in all publications are solely those of the individual author(s) and contributor(s) and not of MDPI and/or the editor(s). MDPI and/or the editor(s) disclaim responsibility for any injury to people or property resulting from any ideas, methods, instructions or products referred to in the content.